Journal of Applied Electrochemistry (2023) 53:1959–1969
https://doi.org/10.1007/s10800-023-01902-2

RESEARCH ARTICLE

Oxygen evolution behavior of $La_{1-x}Sr_xFeO_{3-\delta}$ electrodes in LiCl–KCl melt

Shunichi Kimura[1] · **Takashi Fukumoto**[1] · **Yuta Suzuki**[1] · **Takuya Goto**[1]

Received: 31 January 2023 / Accepted: 25 April 2023 / Published online: 1 June 2023

Abstract

Electrochemical reduction processes of oxides in molten salt have been proposed as the carbon-free technologies in order to achieve carbon neutrality. The anodic behavior of $La_{1-x}Sr_xFeO_{3-\delta}$ as an O_2 evolution anode in LiCl–KCl at 723 K was investigated. The results suggested that at 723 K, the electrical conductivity of $La_{1-x}Sr_xFeO_{3-\delta}$ tended to increase with the Sr doping. The anodic reactions of the $La_{1-x}Sr_xFeO_{3-\delta}$ electrodes were characterized by electrochemical measurements in LiCl–KCl + Li_2O at 723 K. Based on the cyclic voltammograms of the $La_{0.7}Sr_{0.3}FeO_{3-\delta}$ electrode, O_2 evolution has proceeded between 2.7 and 3.6 V. The potential of the $La_{0.7}Sr_{0.3}FeO_{3-\delta}$ electrode during galvanostatic electrolysis has conducted at 39 mA cm^{-2} for 15 h has remained stable at 2.8 V, indicating that the stable evolution of O_2 gas was monitored. The corrosion rate was estimated to have the low value of 8.6×10^{-4} g cm^{-2} h^{-1}. Electrode surface data obtained after electrolysis indicated that the $La_{0.7}Sr_{0.3}FeO_{3-\delta}$ electrode exhibited excellent chemical and physical stability in LiCl–KCl at 723 K. This indicates that the $La_{0.7}Sr_{0.3}FeO_{3-\delta}$ electrode is promising candidate material as inert anodes for oxide decomposition. As an application of the $La_{0.7}Sr_{0.3}FeO_{3-\delta}$ electrode, the electrolytic reduction of CO_2 was also successfully achieved.

Graphical Abstract

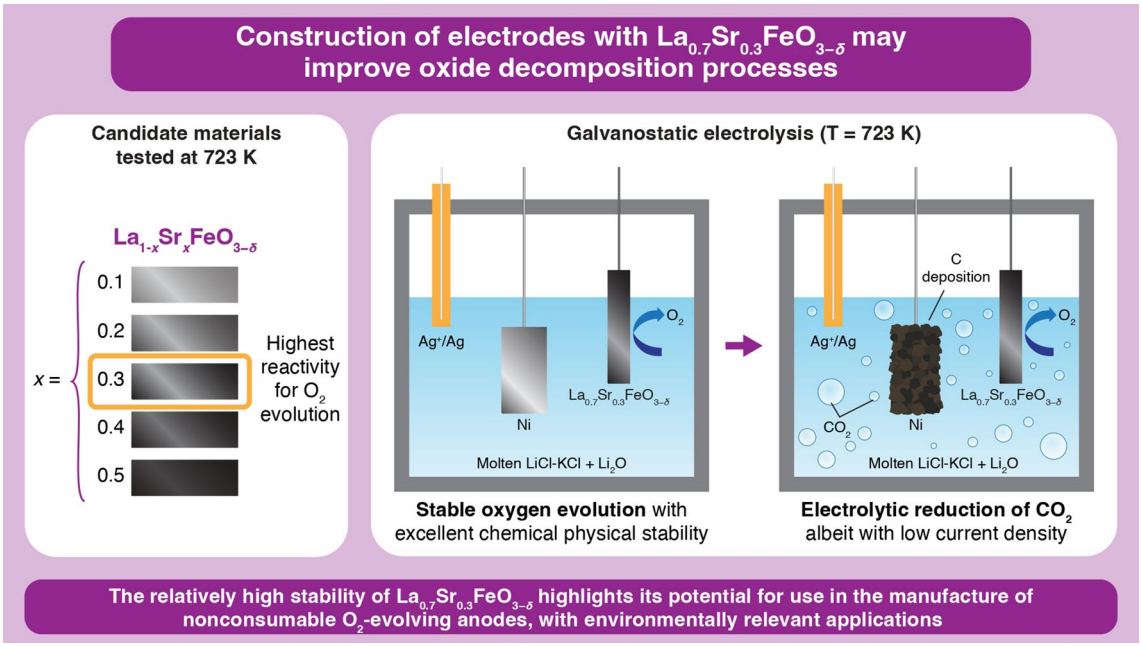

Keywords Molten salt · Inert anode · Electrochemical reduction process · Metal oxide · Carbon free

Extended author information available on the last page of the article

1 Introduction

The electrochemical reduction of metal oxides in molten salt has been proposed as an approach to the production of metals [1-5]. The proposed process of molten salt electrolysis requires the use of an inert anode, as described in the following reactions:

$$\text{In molten salt}: \ MO_x \rightarrow M^{2x+} + xO^{2-} \tag{1}$$

$$\text{Cathode reaction}: \ M^{2x+} + 2xe^- \rightarrow M \tag{2}$$

or

$$MO_x + 2xe^- \rightarrow M + xO^{2-} \tag{3}$$

$$\text{Inert anode reaction}: \ 2O^{2-} \rightarrow O_2 + 4e^- \tag{4}$$

$$\text{Over all cell reaction}: \ MO_x \rightarrow M + x/2O_2 \tag{5}$$

As described above, oxides (MO_x) dissolve into molten salt as cations (M^{2x+}) and oxide ions (O^{2-}). Subsequently, by conducting electrolysis, M^{2x+} is electrochemically reduced to obtain the relevant element in metallic form at the cathode. This element can be alternatively obtained through the direct reduction of MO_x. O^{2-} is electrochemically oxidized such that O_2 gas evolves at the inert anode. However, certain anodic materials that can stably trigger the evolution of O_2 gas stably in molten salt are required because molten salt is highly corrosive.

Carbon anodes have been used in most experiments on the electrochemical reduction of oxides in molten salt. Notably, these anodes react with the evolved O_2 to mainly form CO_2. This reaction has several drawbacks. The carbon anode is gradually consumed and will require to replacement. Importantly, the extent of consumption of the carbon anode significantly exceeds the amount of CO_2 produced, as the said gas originating from the anode tends to erode the electrode. This reduces the current efficiency of the process and increases its energy consumption [6-8]. In this context, the development of nonconsumable O_2-evolving anodes for metal extraction or carbon from oxides (including CO_2) in molten salt is indispensable.

A few materials can act as nonconsumable O_2-evolving anodes in molten salts. The characteristics required of such inert anodes include physical stability at the operating temperature, electrical conductivity, resistance to attack by the molten salt, resistance to attack by chlorine and oxygen gases, resistance to attack by chloride and oxide ions, resistance to thermal shock, and their robustness. Three general types of materials have been investigated as anodic materials for the described process: metals, ceramics, and the cermet electrode. Metal electrodes exhibit high

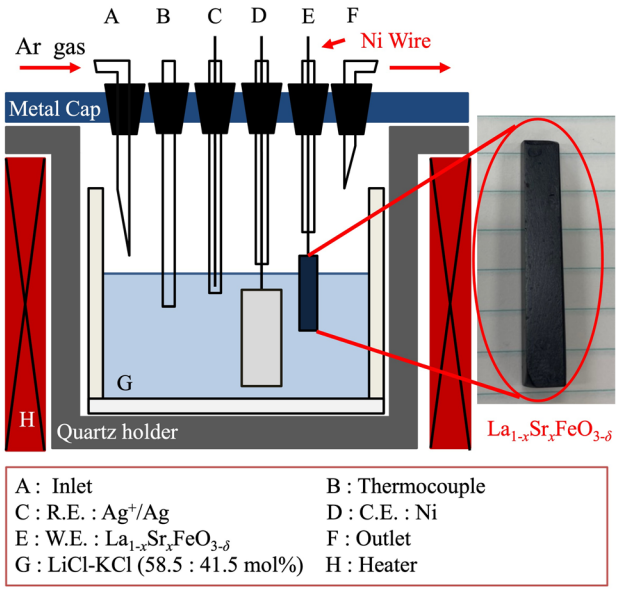

Fig. 1 Configuration of the electrolysis experimental equipment to evaluate the anodic characteristics of the $La_{1-x}Sr_xFeO_{3-\delta}$ electrodes

electrical conductivity and good thermal shock resistance [9-12]. Although metals react with oxygen at high temperatures, the protective oxide layer formed inhibit additional oxidation reactions [9, 10]. Cetain ceramics are known to be stable in molten chlorides. However, the ceramic materials are poor electrical conductors, although a few exhibits semiconducting properties that allow conduction at high temperatures [7, 8, 13, 14]. Studies focusing on ion-conductive ceramics have also been reported [15]. Cermet is a composite material of metal and ceramics, combining the characteristics of both components. The metallic component of cermet has been observed to react with oxygen at high temperatures [16].

In the present study, we focused on valency-controlled metal oxide semiconductors as anodic materials because of their high melting point, excellent resistance to oxidation, excellent thermal stability, and low electrical resistivity at high temperatures. Specifically, the p-type $La_{1-x}Sr_xFeO_{3-\delta}$ semiconductor, which is produced under an O_2 partial pressure of 0.2 atm at a high temperature, was selected for nonconsumable O_2-evolving anodes in molten salt. The p-type $La_{1-x}Sr_xFeO_{3-\delta}$ semiconductor exhibits low electrical resistivity at high temperatures [17]. If parameter x in $La_{1-x}Sr_xFeO_{3-\delta-\delta}$ is 0, $LaFeO_3$ is obtained, which is an insulator at 298 K. The substitution of the trivalent La^{3+} ions by a divalent rare-earth metal, such as Sr^{2+} ions, forces the Fe ions present in the structure to switch from the stable trivalent to the tetravalent states. The coexistence of the trivalent and tetravalent Fe ions causes to an increase in electronic conductivity compared with $LaFeO_3$. $La_{1-x}Sr_xFeO_{3-\delta}$

also exhibits high ionic conductivity due to the formation of additional oxygen vacancies at high temperatures [18, 19].

In this study, we synthesized $La_{1-x}Sr_xFeO_{3-\delta}$ electrodes of various compositions ($x = 0$, 0.1, 0.2, 0.3, 0.4, and 0.5) and then compared their physical properties. Their electrode reactions were characterized by electrochemical measurements, such as cyclic voltammetry. Electrolysis experiments were conducted under different conditions, and the behavior of the anode was evaluated in molten LiCl–KCl at 723 K.

As an application of the $La_{0.7}Sr_{0.3}FeO_{3-\delta}$ electrode, CO_2 electrolysis was performed in a molten LiCl–KCl + 3.0 mol% Li_2O at 723 K. CO_2 decomposition technology will be an effective for combating global warming.

2 Experimental

2.1 Synthesis of $La_{1-x}Sr_xFeO_{3-\delta}$

$La_{1-x}Sr_xFeO_{3-\delta}$ powder was synthesized using the solid phase method. La_2O_3 (99.9%, Kojundo Chemical Laboratory Co., Ltd.), SrO (98.0%, Kojundo Chemical Laboratory Co., Ltd.), and Fe_2O_3 (99.9%, Kojundo Chemical Laboratory Co., Ltd.) were selected as the oxide precursors. Aliquots of the mentioned metal oxide precursors were weighed to obtain mixtures where parameter x assumed the following values: 0.1, 0.2, 0.3, 0.4, and 0.5. The oxides powders were mixed in a mortar and ground using a bead mill (Easy Nano RMB; Aimex Co., Ltd.) with ZrO_2 balls (φ2 mm) at 2000 rpm in ethanol. The milled powders were examined using a particle size analyzer (SALD-2300; Shimadzu Co., Ltd.) to keep the average particle sizes less than 1 µm. Afterward, the milled powders were then pressed using a 50 mm × 10 mm metal mold at 70 MPa and a cold isostatic press (CIP; Dr.CIP, Kobe Steel Co., Ltd.) at 245 MPa. The formed pellets were sintered in the range of 1473–1723 K for 8 h under the O_2 partial pressure of 0.2 atm. The surfaces of the obtained $La_{1-x}Sr_xFeO_{3-\delta}$ pellets were mechanically polished, first with SiC paper, then with diamond particles (below a size of 6 µm) prior to characterization. The image of a pellet is shown in Fig. 1. A 50 mm × 10 mm × 10 mm metal mold was used. However, the size of the sintered body was subject to shrinking because of the CIP and sintering process. The size of the sintered pellets was measured after the sintering process to be in the range of 46–48 mm × 8–9 mm × 8–9 mm.

The density of the $La_{1-x}Sr_xFeO_{3-\delta}$ pellets was determined using the Archimedes technique. The polished surfaces of the pellets were investigated by scanning electron microscopy (SEM; JSM-7001FD, JEOL Ltd.) and energy-dispersive X-ray spectroscopy (EDS; JED-2300, JEOL Ltd.). The crystal structures of the pellets were characterized by X-ray diffraction (XRD; RINT-2001 MultiFlex, Rigaku Co, Ltd.). Sample identification was achieved using the relevant diffraction pattern, and the average lattice constant was calculated. The thermoelectric properties of the $La_{1-x}Sr_xFeO_{3-\delta}$ pellets were measured from room temperature to 1073 K using a four-terminal conductivity analyzer (RZ2001i, Ozawa Science Co, Ltd.).

2.2 Electrochemical measurements

Figure 1 shows a schematic view of the electrolytic apparatus used. A quartz holder comprising high-purity silica was used. The working electrode comprised a $La_{1-x}Sr_xFeO_{3-\delta}$ electrode mirror-polished using diamond particles (below a size of 6 µm). Pt wire was used to connect the $La_{1-x}Sr_xFeO_{3-\delta}$ electrode. The counter electrode was Ni wire in a spiral shape (99.35%, φ1.0 mm, Sumiden Fine Conductors Co., Ltd.). The reference electrode was an Ag wire immersed in a eutectic LiCl–KCl melt containing 1 mol% AgCl in a thin-bottomed alumina tube. The alumina tube was sufficiently thin enough to use the membrane of the reference because the alumina intrinsically included a small quantity of various metal ions, which afforded ion conductivity at the experimental temperatures. The potential of the reference electrode was calibrated in reference to that of the Li^I | Li electrode, which was prepared by electrodepositing Li metal on a nickel electrode.

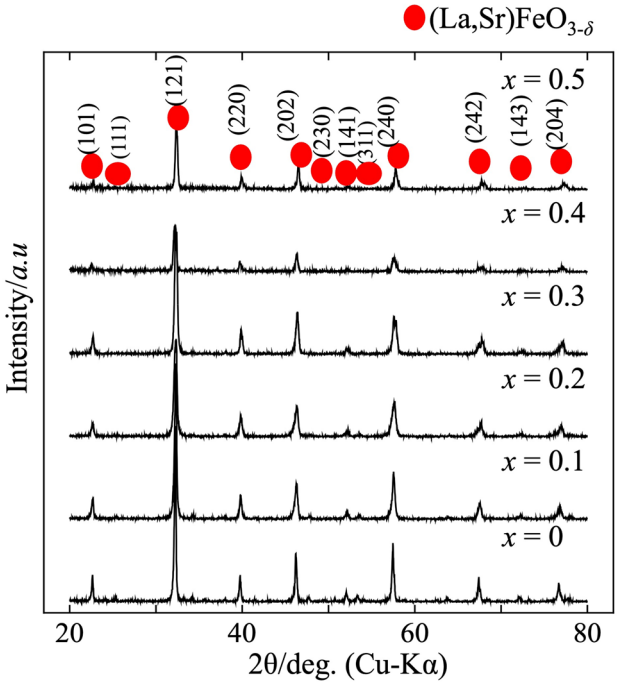

Fig. 2 X-ray diffraction patterns of $La_{1-x}Sr_xFeO_{3-\delta}$ samples after sintering at 1498–1723 K for 8 h in atmospheric air ($x = 0$, 0.1, 0.2, 0.3, 0.4, and 0.5 at 1723, 1623,1623, 1623, 1523, and 1498 K, respectively)

Lithium chloride (LiCl, 99.0%, Fujifilm Wako Pure Chemical Co.) and potassium chloride (KCl, 99.5%, Fujifilm Wako Pure Chemical Co.) were mixed in a eutectic composition (58.5 mol% LiCl, 41.5 mol% KCl). The obtained mixture was dried under vacuum conditions for more than 24 h at 473 K to remove water from it. The eutectic mixture was prepared to a total weight of 200 g (LiCl, 89.0 g; KCl, 111.0 g). Thereafter, it was melted in a high-purity alumina crucible. Lithium oxide (Li_2O, 99.5%, Fujifilm Wako Pure Chemical Co.) was used as the source of the oxide ion and was directly added to the melt. The experimental processes were conducted in a glove box under dried argon atmosphere. Thus, the effect of moisture was practically negligible.

CO_2 electrolysis was performed in LiCl–KCl + 3.0 mol% Li_2O at 723 K. The cathode deposits after CO_2 electrolysis were analyzed by Raman spectroscopy analysis (NRS-5500, Jasco Co.) using a YAG laser (532 nm).

3 Results and discussion

3.1 Synthesis of $La_{1-x}Sr_xFeO_{3-\delta}$

$La_{1-x}Sr_xFeO_{3-\delta}$ powder was synthesized using the solid phase method. La_2O_3, SrO, and Fe_2O_3 powders were selected as oxide precursors. $LaFeO_3$ comprises stable trivalent La and trivalent Fe, and it exhibits a perovskite crystal structure. $La_{1-x}Sr_xFeO_{3-\delta}$ was synthesized by replacing the trivalent La ion with the divalent Sr ions, forcing the Fe ion to switch from the stable trivalent to the tetravalent states [18, 19].

$$(1-x)\,La_2O_3 + 2xSrO + \alpha\text{ - }Fe_2O_3 \rightarrow 2\,La_{1-x}Sr_xFeO_{3-\delta} \quad (6)$$

The oxide precursors of $La_{1-x}Sr_xFeO_{3-\delta}$ were weighed such that values of $x = 0$, 0.1, 0.2, 0.3, 0.4, and 0.5 were obtained for parameter x, and the obtained mixtures were ground using a bead mill and pressed using a CIP at 245 MPa. Subsequently, the formed pellets were sintered within the range of 1473–1623 K for 8 h under the O_2 partial pressure of 0.2 atm. Figure 2 shows the XRD spectra of the $La_{1-x}Sr_xFeO_{3-\delta}$ samples obtained after the mentioned sintering process. The XRD patterns of the $La_{1-x}Sr_xFeO_{3-\delta}$ samples ($x = 0$, 0.1, 0.2, 0.3, 0.4, and 0.5) were indicative of single-phase (La, Sr) $FeO_{3-\delta}$ ceramics. The average lattice constants of the samples were calculated from the relevant XRD spectra calibrated using a reference sample (pure Si). The axis average lattice constants for the a-, b-, and c-axes of the $La_{1-x}Sr_xFeO_{3-\delta}$ samples decreased with an increasing in parameter x. The values of the coefficient (R^2) of each axis were calculated using a regression line to be 0.8632, 0.9595, and 0.8830 for the a-, b-, and c-axes, respectively (Fig. S1, supplementary information). The coefficient (R^2) exceeded 0.85 for the three axes. The average lattice constants of the synthesized $La_{1-x}Sr_xFeO_{3-\delta}$ semiconductors were confirmed to be correlated with the parameter x of $La_{1-x}Sr_xFeO_{3-\delta}$.

The coexistence of Fe^{3+} and Fe^{4+} ion was achieved by substituting La^{3+} for Sr^{2+} [20]. As the ionic radius of Fe^{4+} is smaller than that of Fe^{3+}, the average lattice constant decreased with an increase in parameter x (Fig. S1).

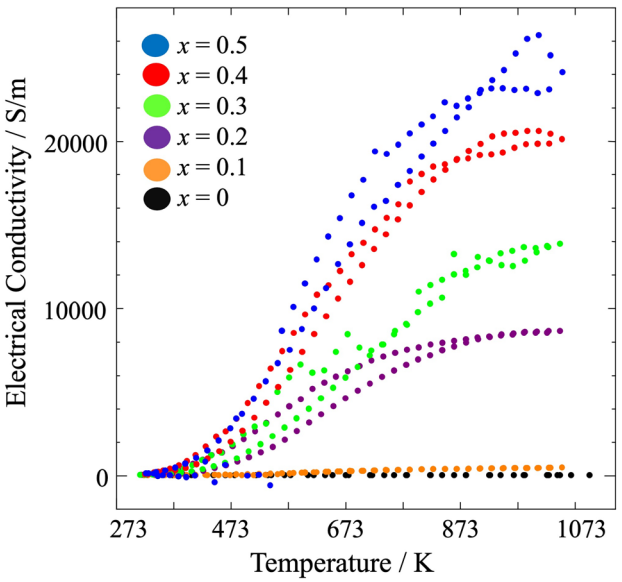

Fig. 3 Relationship between x and the electrical conductivity of the $La_{1-x}Sr_xFeO_{3-\delta}$ electrodes

Table 1 Relationship between the sintering temperature and density of $La_{1-x}Sr_xFeO_{3-\delta}$

	Sintering temperature (K)								
	1473	1498	1523	1548	1573	1623	1648	1673	1723
Density of $LaFeO_3$ (g cm^{-3})	–	–	–	–	–	6.2230	–	6.2877	6.3189
Density of $La_{0.9}Sr_{0.1}FeO_{3-\delta}$ (g cm^{-3})	–	–	–	–	5.6859	6.4289	6.4320	6.4398	–
Density of $La_{0.9}Sr_{0.1}FeO_{3-\delta}$ (g cm^{-3})	–	–	–	–	5.8779	6.3994	6.3353	Melt	–
Density of $La_{0.7}Sr_{0.3}FeO_{3-\delta}$ (g cm^{-3})	–	–	–	–	5.9317	6.2820	Melt	–	–
Density of $La_{0.6}Sr_{0.4}FeO_{3-\delta}$ (g cm^{-3})	–	6.0836	6.0898	6.0775	Melt	–	–	–	–
Density of $La_{0.5}Sr_{0.5}FeO_{3-\delta}$ (g cm^{-3})	5.9220	5.9640	5.9580	Melt	–	–	–	–	–

Therefore, the formation of a substituted $La_{1-x}Sr_xFeO_{3-\delta}$ solid solution was suggested.

3.2 Densification of $La_{1-x}Sr_xFeO_{3-\delta}$

The ceramic electrodes used for molten salt electrolysis need to be characterized by high density. In this study, the $La_{1-x}Sr_xFeO_{3-\delta}$ samples with different x values ($x=0$, 0.1, 0.2, 0.3, 0.4, and 0.5) were sintered at various temperatures in the range of 1473–1723 K, to determine the most suitable sintering temperature for the densification of the samples. Notably, the densities (g cm^{-3}) were measured using the Archimedes technique.

Table 1 shows the relationship between the sintering temperature and density of $La_{1-x}Sr_xFeO_{3-\delta}$. The densities of the Sr-doped samples with $x=0.1$, 0.2, and 0.3 drastically increased at 1623 K. Contrarily, the densities of the Sr-doped samples with $x=0.4$ and 0.5 reached a maximum at 1523 and 1498 K. As confirmed from the binary phase diagram of $LaFeO_3$–$SrFeO_{3-\delta}$ [21], the melting point tended to decrease as the Sr concentration (x) increased. Thus, the densification temperature decreased as the x value increased.

3.3 Electrical properties of $La_{1-x}Sr_xFeO_{3-\delta}$

Figure 3 shows data reflecting the electrical properties of the $La_{1-x}Sr_xFeO_{3-\delta}$ samples characterized by the highest density for each composition ratio at various temperatures. The conductivities of each sample were measured using the four-terminal conductivity analyzer from room temperature to 1073 K. When the Sr composition ratio was changed from $x=0$ to $x=0.5$, at 723 K, the electrical conductivity of the material increased from 5.7×10^{-1} to 1.6×10^{4} S/m. The substitution of trivalent La^{3+} ion by a divalent metal, such as Sr^{2+} ion, forced the Fe ion to switch from the stable trivalent to the tetravalent states. The coexistence of the trivalent and tetravalent Fe ions caused to an increase in electronic conductivity compared with the $LaFeO_3$ of the parent material. Furthermore, $La_{1-x}Sr_xFeO_{3-\delta}$ ($x>0.1$) also exhibits higher ionic conductivity than $LaFeO_3$ owing to the formation of additional oxygen vacancies at elevated temperatures [19, 22].

3.4 Electrochemical behavior of oxide ions on $La_{1-x}Sr_xFeO_{3-\delta}$ electrodes

Cyclic voltammetry performed in a LiCl–KCl melt at 723 K to investigate the electrochemical behavior of oxide ions on the $La_{0.7}Sr_{0.3}FeO_{3-\delta}$ electrode. Figure 4 shows the cyclic voltammograms obtained using the $La_{0.7}Sr_{0.3}FeO_{3-\delta}$ electrode before and after the addition of Li_2O to the LiCl–KCl melt to final concentrations of 0.5 and 3.0 mol%. Notably, the solubility of Li_2O in the LiCl–KCl melt at 723 K has been reported to be approximately 1.0 mol% [23]. The optimal amount of Li_2O was selected to be 3.0 mol% to maintain the saturation of Li_2O in the molten salt during electrolysis.

Before the addition of Li_2O to the LiCl–KCl melt, the oxidation current density began to increase at a value for the potential of 3.7 V. Contrarily, after the addition of Li_2O,

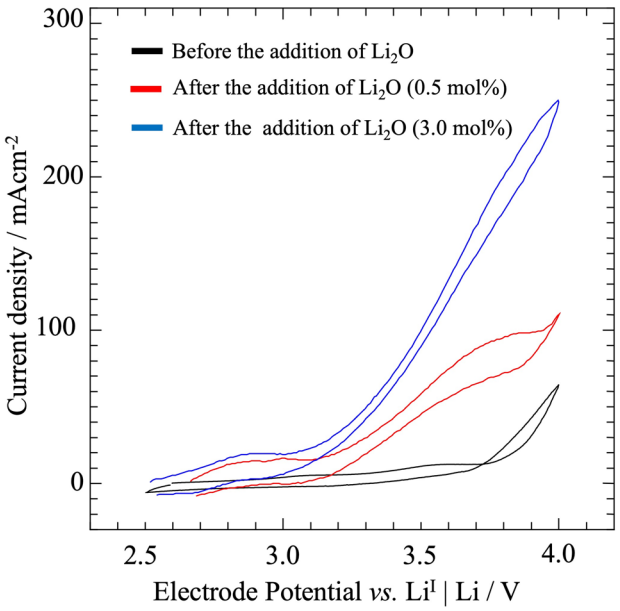

Fig. 4 Cyclic voltammograms of the $La_{0.7}Sr_{0.3}FeO_{3-\delta}$ electrode in LiCl–KCl melts at 723 K. Scan rate: 100 mV s^{-1}

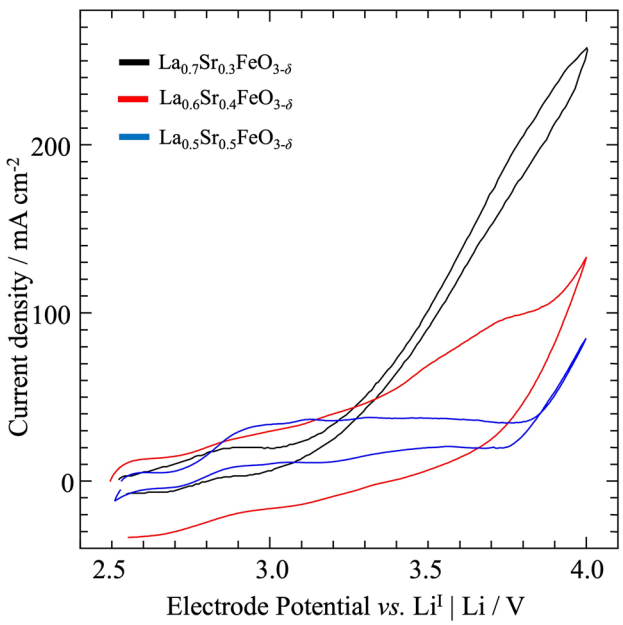

Fig. 5 Cyclic voltammograms of $La_{1-x}Sr_xFeO_{3-\delta}$ electrodes recorded at 723 K in LiCl–KCl melts containing Li_2O 3.0 mol%. Scan rate: 100 mV s^{-1}

the oxidation current density began to increase at a potential of 2.7 V. In previous studies [24, 25] conducted on the same electrolyte comprising molten LiCl–KCl and Li_2O, which included a boron-doped diamond electrode acting as the anode, O_2 and Cl_2 evolution was observed to proceed at 2.5 and 3.6 V, respectively. Therefore, in the present system with a $La_{0.7}Sr_{0.3}FeO_{3-\delta}$ electrode as the anode, the increase in oxidation current density at 3.7 V observed before the addition of Li_2O to the LiCl–KCl melt was attributed to the reaction leading to chlorine gas evolution or chlorine compounds. Contrarily, the increase in oxidation current density at 2.7 V observed after the addition of Li_2O was attributed to the reaction leading to O_2 gas evolution. In the LiCl–KCl melt containing Li_2O, O_2 gas evolution was assumed to occur between 2.7 and 3.6 V at 723 K.

The electrochemical behavior of oxide ions on the $La_{1-x}Sr_xFeO_{3-\delta}$ electrode ($x = 0.3$, 0.4, and 0.5) was also investigated by comparing the cyclic voltammograms obtained at each x value, to determine the composition of the $La_{1-x}Sr_xFeO_{3-\delta}$ electrode that affords the highest reactivity leading to O_2 evolution. Figure 5 shows the cyclic voltammograms of $La_{1-x}Sr_xFeO_{3-\delta}$ electrodes ($x = 0.3$, 0.4, and 0.5) in the LiCl–KCl melt containing 3.0 mol% Li_2O at 723 K. The electrode surface area was defined as the geometric surface area. The different background currents shown in Fig. 5 were attributed to the differences in the real surface area. As shown in Fig. 3, these three electrodes ($x = 0.3$, 0.4, and 0.5) exhibited the highest electrical conductivity. The $La_{0.5}Sr_{0.5}FeO_{3-\delta}$ electrode exhibited the highest oxidation current density between 2.8 and 3.1 V, but the $La_{0.7}Sr_{0.3}FeO_{3-\delta}$ electrode exhibited the highest oxidation current density between 3.2 and 3.6 V (Fig. 5). The current density (Fig. 5) of $La_{0.5}Sr_{0.5}FeO_{3-\delta}$ electrode practically remained constant from 2.9 to 3.4 V. In a study by Kado et al. [25], the oxidation current between 2.5 and 3.6 V in LiCl–KCl at 723 K was due to O_2 generation. Therefore, the shape of the cyclic voltammograms of each electrode suggested that the O_2 evolution reaction on $La_{0.7}Sr_{0.3}FeO_{3-\delta}$ and $La_{0.6}Sr_{0.4}FeO_{3-\delta}$ were governed by the charge-transfer step, whereas that on $La_{0.5}Sr_{0.5}FeO_{3-\delta}$ was governed by the diffusion step. The differences in the shape of the cyclic voltammograms were due to differences in the O_2 evolution processes on the electrode/the molten salt interface. The different amounts of Sr added to $La_{1-x}Sr_xFeO_{3-\delta}$ affected the catalytic activity of the O_2 evolution reaction.

We decided to use the $La_{0.7}Sr_{0.3}FeO_{3-\delta}$ electrode in electrolysis tests. This electrode exhibited the lowest electrical conductivity during the cyclic voltammetry experiments. This confirmed that an increase in electrical conductivity did not necessarily enhance the O_2 evolution reaction.

3.5 Electrolysis tests performed using the $La_{0.7}Sr_{0.3}FeO_{3-\delta}$ electrode

Based on the cyclic voltammetry results, the O_2 evolution process was concluded to have occurred between 2.7 and 3.6 V in the LiCl–KCl melt containing 3.0 mol% Li_2O at 723 K. Figure 6 shows the time transition of current densities measured during potentiostatic electrolysis experiments conducted at 2.9 V, 3.3 V, and 3.5 V. The anodic currents

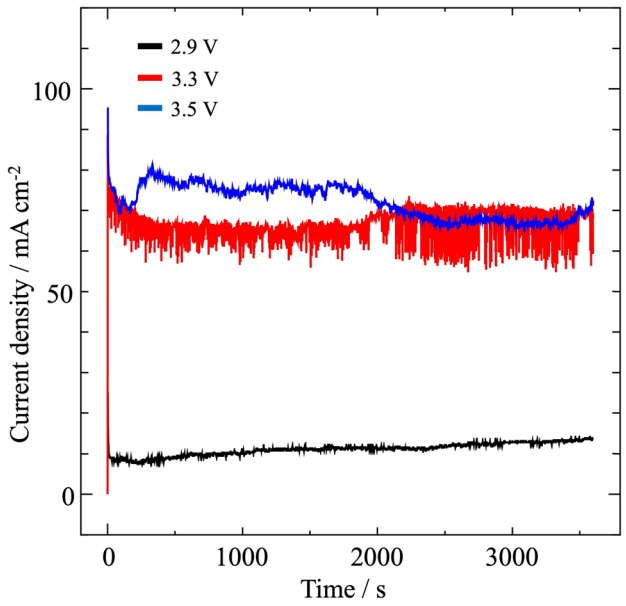

Fig. 6 Time transition of current densities on the $La_{0.7}Sr_{0.3}FeO_{3-\delta}$ electrode at 2.9, 3.3, and 3.5 V for 1 h

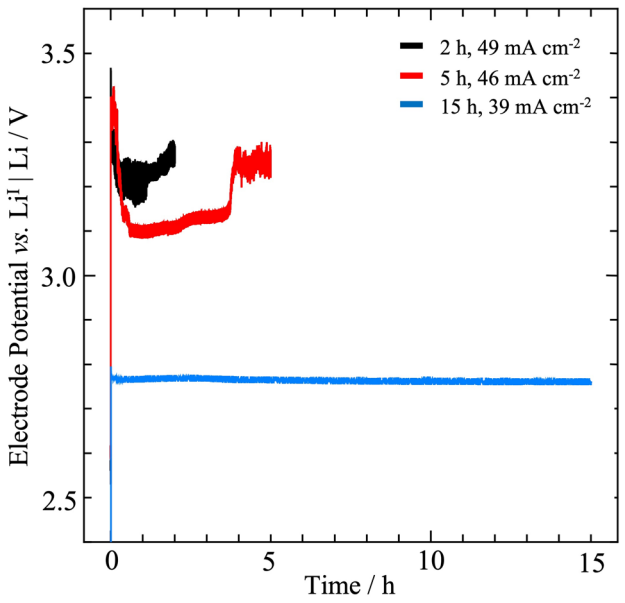

Fig. 7 Variation of potentials on the $La_{0.7}Sr_{0.3}FeO_{3-\delta}$ electrode at 50 mA cm^{-2} for 2, 5, and 15 h

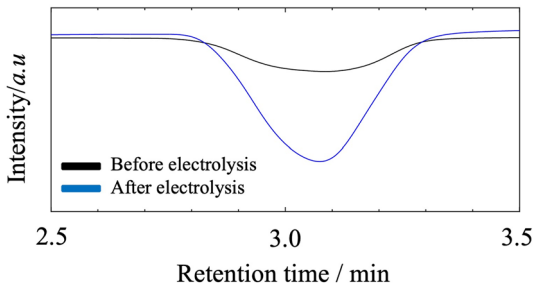

Fig. 8 Gas chromatogram of gas samples collected before and after galvanostatic electrolysis conducted at a current density of 39 mA cm^{-2} for 15 h

measured in association with the O_2 gas evolution process practically remained steady around 10 mA cm^{-2} at 2.9 V and around 70 mA cm^{-2} at 3.3 V and 3.5 V. This implied that the electrochemical reaction taking place at the $La_{0.7}Sr_{0.3}FeO_{3-\delta}$ electrode did not change during electrolysis. The current density fluctuation shown in Fig. 6 was caused by altering the electrode surface area because of the adsorption and desorption of O_2 gas bubbles evolved at the electrode/molten salt interface during the experiment.

The electrolysis conditions were selected based on Fig. 4. The O_2 evolution process was observed at the potentials ranging from 2.7 to 3.6 V in the LiCl–KCl melt containing 3.0 mol% Li_2O at 723 K. The current density corresponding to the potential range of the gas evolution was selected from 10 to 100 mA cm^{-2} depending on the experiment. Figure 7 shows data on the time transition of the potential during galvanostatic electrolysis experiments conducted at current densities of 49, 46, 39 mA cm^{-2} for 2, 5, 15 h, respectively. The potential at which the O_2 gas evolution process occurred fluctuated between 3.1 and 3.3 V during the experiments conducted at 49 and 46 mA cm^{-2} for 2 and 5 h, respectively. For the galvanostatic electrolysis at 39 mA cm^{-2}, the potential remained stable at 2.8 V during the electrolysis (Fig. 7). Oppositely, as the currents density exceeded 39 mA cm^{-2},

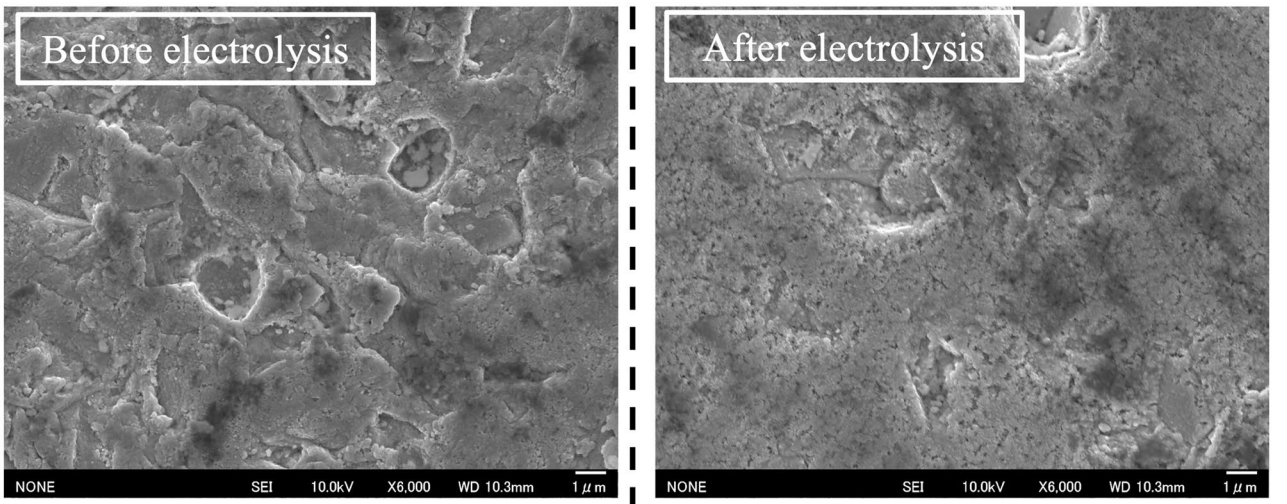

Element	Concentration (%)
O	55.4
C	5.7
La	15.2
Sr	5.1
Fe	18.6

Element	Concentration (%)
O	55.0
C	7.7
La	15.6
Sr	4.3
Fe	17.4

Fig. 9 Scanning electron microscopy images and energy-dispersive X-ray spectroscopy results of the surface of the $La_{0.7}Sr_{0.3}FeO_{3-\delta}$ electrode before and after electrolysis at 39 mA cm^{-2} for 15 h

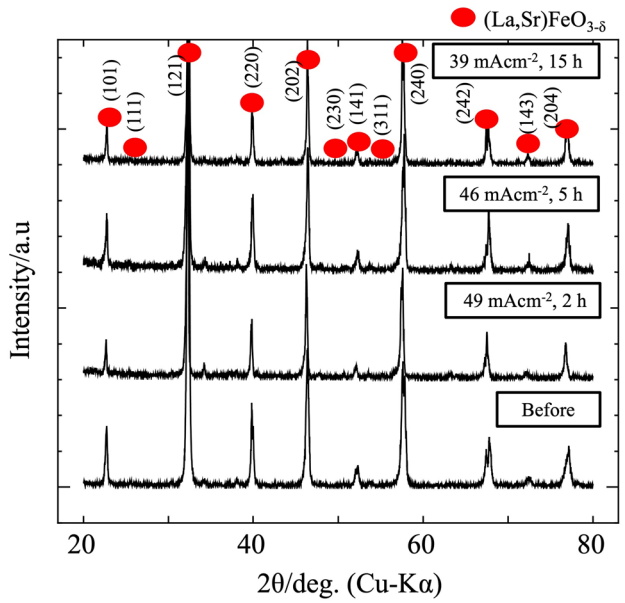

Fig. 10 X-ray diffraction patterns of the $La_{0.7}Sr_{0.3}FeO_{3-\delta}$ electrode recorded before and after the galvanostatic electrolysis

the potential began to fluctuate. Therefore, an applied current density of 39 mA cm^{-2} was chosen for the experiment.

The mechanism of the fluctuating potential shown in Fig. 7 was unclear. A possible explanation was that the effect of potential dependence on the behavior of the nucleation, growth, and detachment of O_2 gas on the electrode might have caused the difference in the current time transition.

In addition, the gas generated on the $La_{0.7}Sr_{0.3}FeO_{3-\delta}$ electrode during the electrolysis conducted at a current density of 39 mA cm^{-2} for 15 h was analyzed by gas chromatography (GC-2014, Shimadzu Co, Ltd.). Figure 8 shows the gas chromatograms of gas samples collected before and after galvanostatic electrolysis. It was confirmed in advance that the peak attributed to O_2 gas had a retention time of approximately 3 min based on the results of injecting O_2 standard gas. Figure 8 shows that the intensity of the peak due to O_2 in the gas sample collected after electrolysis was increased. Based on the gas chromatograms, the current efficiency of the O_2 evolution reaction (Eq. 4) was estimated at 30.4%. The following reactions are also one possible explanation for the low current efficiency of O_2 gas. Oxide ion (O^{2-}) was oxidized to form intermediate species (for example, O_2^{2-}, O_2^{-}, and O^{-}):

$$2O^{2-} \rightarrow O_2^{2-} + 2e^- \quad (7)$$

$$2O^{2-} \rightarrow O_2^{-} + 3e^- \quad (8)$$

$$O^{2-} \rightarrow O^{-} + e^- \quad (9)$$

These intermediates formed by the anodic reactions suppressed the current efficiency and the subsequent reactions should occur.

$$O_2^{2-} \rightarrow O_2^{-} + e^- \quad (10)$$

$$O^{2-} + O^{-} \rightarrow O_2^{2-} + e^- \quad (11)$$

In addition, certain intermediates decomposed to form O and O^{2-} [26], and the atomic oxygen easily reacted with the metal wire in the cell.

$$O_2^{-} \rightarrow O + O^{2-} \quad (12)$$

The jump in potential led by the small increase in current density (Fig. 7) might also have been caused by changes in side reactions associated with O_2 ions, such as those in Eqs. (7)–(12). The relatively low electric conductivity of the $La_{0.7}Sr_{0.3}FeO_{3-\delta}$ (Fig. 3) may be another reason for the suppressed the current efficiency.

The sample subjected to electrolysis at 39 mA cm^{-2} current density for 15 h had the longest time and highest total electrolysis charge in this study. The morphological surface changes exhibited by the $La_{0.7}Sr_{0.3}FeO_{3-\delta}$ electrode because of the electrolysis experiment were investigated by SEM, EDS, and XRD. Figure 9 shows the SEM images of the electrode surfaces and the results of the EDS elemental analyses conducted on the electrodes before and after electrolysis. The SEM images revealed tiny holes (several tens of nanometers) in the surface morphology after electrolysis. It was suggested that the tiny holes were produced by eroding the anode during O_2 evolution. The EDS results confirmed that there were practically no change in the elemental composition. The detected carbon

Table 2 Corrosion rate and weight change of the $La_{0.7}Sr_{0.3}FeO_{3-\delta}$ electrode in association with the performance of galvanostatic electrolysis, conducting electric quantity of $La_{0.7}Sr_{0.3}FeO_{3-\delta}$ electrode

Conditions of the galvanostatic electrolysis (current density, time)	Total electrolysis charge (C)	Weight change (g)	Corrosion rate (g cm^{-2} h^{-1})
49 mA cm^{-2}, 2 h	576	0	0
46 mA cm^{-2}, 5 h	901	−0.004	2.4×10^{-4}
39 mA cm^{-2}, 15 h	2970	−0.0181	8.6×10^{-4}

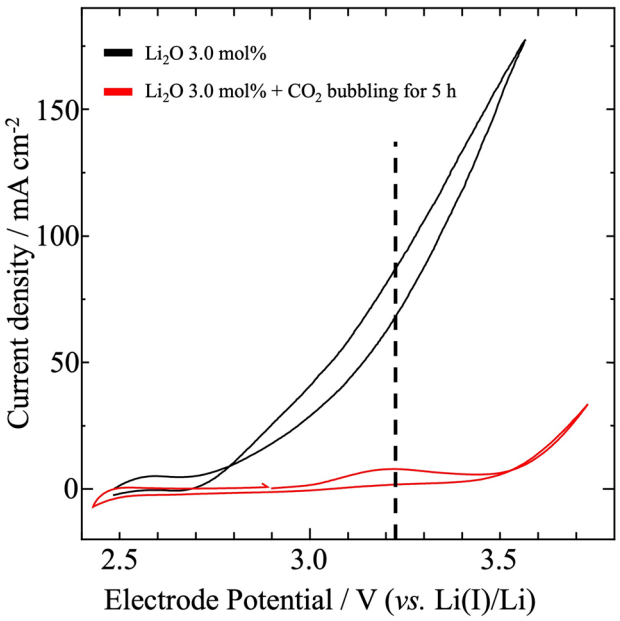

Fig. 11 Cyclic voltammograms of electrochemical reaction before and after CO_2 bubbling for 5 h at 723 K. Scan rate: 10 mV s^{-1}

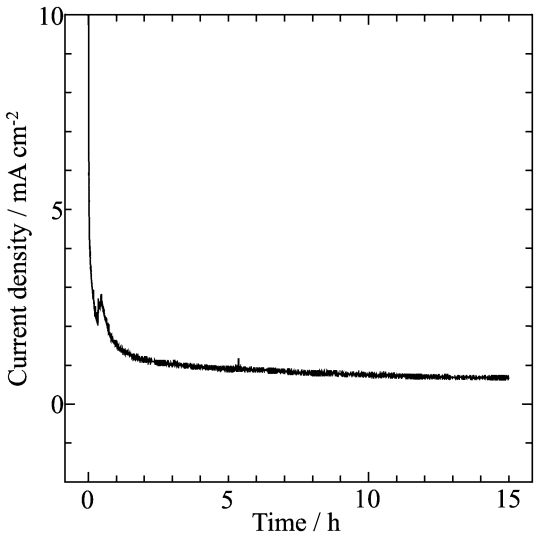

Fig. 12 Time transition of current densities on the $La_{0.7}Sr_{0.3}FeO_{3-\delta}$ electrode at 3.23 V for 15 h

attributed to carbon tape which was used to bond the samples to the observation table during SEM.

Figure 10 shows the XRD patterns of the $La_{0.7}Sr_{0.3}FeO_{3-\delta}$ electrode recorded before and after galvanostatic electrolysis experiments. A single-phase diffraction pattern attributed to (La,Sr)$FeO_{3-\delta}$ was observed in all the samples of before and after galvanostatic electrolysis experiments. The lack of change in the diffraction pattern before and after galvanostatic electrolysis indicated that the crystal structure of the (La,Sr)$FeO_{3-\delta}$ electrode had

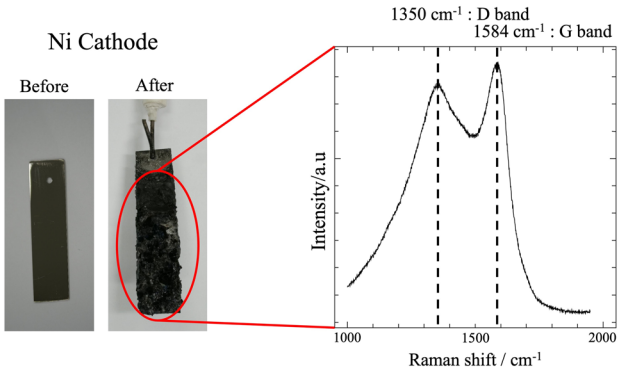

Fig. 13 Image of the Ni cathode before and after electrolysis and Raman spectra of electrodeposition

not changed. The $La_{0.7}Sr_{0.3}FeO_{3-\delta}$ electrode showed high corrosion resistance. As a mechanism for the high corrosion resistance, it is suggested that the $La_{0.7}Sr_{0.3}FeO_{3-\delta}$ electrode itself functions as an oxide protective layer. The $La_{0.7}Sr_{0.3}FeO_{3-\delta}$ electrode exhibited sufficient chemical and physical stability for use in molten salt electrolysis experiments.

The corrosion rate γ is another important property that defines the suitability of nonconsumable O_2-evolving anodes. In this study, the value of parameter γ (g cm^{-2} h^{-1}) was estimated using Eq. (13) [8]:

$$\gamma = \Delta W / t \cdot S \tag{13}$$

where ΔW is the difference between the weight (g) of the anode before and after electrolysis, t is the electrolysis time (h), and S is the surface area of the part of the electrode that is immersed in the electrolyte. The corrosion evaluation of the anode during galvanostatic electrolysis was conducted in a LiCl–KCl melt containing 3.0 mol% Li_2O at 723 K. The conditions are summarized in Table 2.

As shown in Table 2, the corrosion rate of the $La_{0.7}Sr_{0.3}FeO_{3-\delta}$ electrode was calculated to have a value between 0 and 8.6×10^{-4} g cm^{-2} h^{-1}. Considering that the weight loss of $La_{0.7}Sr_{0.3}FeO_{3-\delta}$ was not confirmed after immersion for 10 h without electrolysis in LiCl–KCl at 723 K (Table S1), the calculated values in Table 2 were the corrosion rate due to electrolytic corrosion. The weight loss of this anode was caused by eroding the anode during O_2 evolution because tiny holes (several tens of nanometers) in the surface morphology was observed in the SEM images for the sample after electrolysis at 39 mA cm^{-2} for 15 h (Fig. 9). Fray et al. [8] deemed an anode inert as long as the value of the corrosion rate was below 1.5×10^{-3} g cm^{-2} h^{-1}. Therefore, $La_{0.7}Sr_{0.3}FeO_{3-\delta}$ is an extremely promising candidate in the manufacture of

nonconsumable O_2-evolving anodes for metal oxides or CO_2 decomposition.

3.6 CO_2 decomposition using the $La_{0.7}Sr_{0.3}FeO_{3-\delta}$ electrode

Cyclic voltammetry experiments were performed in a LiCl–KCl melt + 3.0 mol% Li_2O after CO_2 bubbling for 5 h at 723 K. Figure 11 shows the cyclic voltammograms recorded before and after the CO_2 bubbling for 5 h. The oxidation current density after CO_2 bubbling was smaller than before CO_2 bubbling. The reaction shown in Eq. (14) proceeded by CO_2 bubbling in an electrolytic bath.

$$CO_2 + O^{2-} \rightarrow CO_3^{2-} \tag{14}$$

The decrease in oxide ions in the electrolytic bath led to a decrease in current density due to the O_2 evolution reaction (Eq. 4).

Potentiostatic electrolysis was performed at 3.23 V, the peak of oxidation current density.

Figure 12 shows the time transition of current densities measured during potentiostatic electrolysis experiments at 3.23 V. The anodic currents measured in association with the O_2 gas evolution process practically remained steady at 1 mA cm^{-2}.

Black deposition observed on the Ni cathode after the 15 h electrolysis was analyzed by Raman spectroscopy. Figure 13 shows the Raman spectra of the electrodeposition. Two peaks attributed to carbon were confirmed at 1350 cm^{-1} and 1584 cm^{-1}. The following cathodic reaction proceeded.

$$CO_3^{2-} + 4e^- \rightarrow C + 3O^{2-} \tag{15}$$

CO_2 electrolysis was successfully achieved. However, the current density of the electrolysis was low in the present experimental system; therefore, the electrolysis bath requires improvement.

4 Conclusion

Dense $La_{1-x}Sr_xFeO_{3-\delta}$ ceramic materials of different compositions ($x = 0.1$, 0.2, 0.3, 0.4, and 0.5) were obtained through a sintering process between 1498 and 1673 K for 8 h under an O_2 the partial pressure of 0.2 atm. The electrical conductivity of the $La_{1-x}Sr_xFeO_{3-\delta}$ ceramics increased from 5.7×10^{-1} to 1.6×10^4 S/m as x increased from 0 to 0.5.

The suitability of the $La_{1-x}Sr_xFeO_{3-\delta}$ electrodes for use as O_2-evolving anodes was investigated through a series of electrochemical measurements in LiCl–KCl melt containing Li_2O at 723 K. The cyclic voltammetry experiments were conducted on the $La_{1-x}Sr_xFeO_{3-\delta}$ electrodes with $x = 0.3$, 0.4, and 0.5. The $La_{0.5}Sr_{0.5}FeO_{3-\delta}$ electrode exhibited the highest oxidation current density between 2.8 and 3.1 V, whereas the $La_{0.7}Sr_{0.3}FeO_{3-\delta}$ electrode exhibited the highest oxidation current density between 3.2 and 3.5 V. The current density of the $La_{0.5}Sr_{0.5}FeO_{3-\delta}$ electrode shown in Fig. 5 practically remained constant from 2.9 to 3.4 V, indicating that the O_2 evolution was governed by a diffusion control. As the applied potential range was equal to from 0.4 to 1.0 V expressed by overpotential, the applied potentials were far from the equilibrium potential of O_2 generation [25].

The $La_{0.7}Sr_{0.3}FeO_{3-\delta}$ electrode was subjected to electrolysis tests and exhibited the lowest electrical conductivity among the electrodes used in the cyclic voltammetry experiments. This confirmed that increases in electrical conductivity were not necessarily associated with enhancements of the reaction leading to O_2 gas evolution.

During galvanostatic electrolysis, the potential of the $La_{0.7}Sr_{0.3}FeO_{3-\delta}$ electrode remained stable between 2.8 and 3.3 V, regardless of the reaction conditions. Based on the gas chromatography results, the stable evolution of O_2 gas was confirmed to have occurred, and the current efficiency of the electrolysis process conducted at 39 mA cm^{-2} current density for 15 h was estimated at 30.4%. The corrosion rate of $La_{0.7}Sr_{0.3}FeO_{3-\delta}$ was estimated at a very low value of 8.6×10^{-4} g cm^{-2} h^{-1}. The XRD, SEM, and EDS results of the $La_{0.7}Sr_{0.3}FeO_{3-\delta}$ electrode before and after the electrolytic process showed that the electrode exhibited excellent chemical and physical stability in the LiCl–KCl melts containing Li_2O at 723 K. This study shows that $La_{0.7}Sr_{0.3}FeO_{3-\delta}$ is a promising candidate material for the manufacture of nonconsumable O_2-evolving anodes.

As an application of the $La_{0.7}Sr_{0.3}FeO_{3-\delta}$ electrode, CO_2 electrolysis was successfully achieved. However, the current density of the CO_2 electrolysis was low in the present experimental system; therefore, the electrolysis bath and electrode require improvement.

Supplementary Information The online version contains supplementary material available at https://doi.org/10.1007/s10800-023-01902-2.

Author contributions Shunichi Kimura wrote the main manuscript text. Takashi Fukumoto and Yuta Suzuki prepared figures 11-13. Takuya Goto planned the concept of this study. All authors reviewed the manuscript.

Declarations

Competing interests On behalf of all authors, the corresponding author states that there is no conflict of interest.

References

1. Allanore A, Yin L, Sadoway DR (2013) Nature 497:353–356
2. Chen GZ, Fray DJ, Farthing TW (2000) Nature 407:361–364
3. Suzuki RO, Aizawa M, Ono K (1999) J Alloys Compd 288:173–182
4. Sakamura Y, Kurata M, Inoue T (2006) J Electrochem Soc 153:D31–D39
5. Nohira T, Yasuda K, Ito Y (2003) Nat Mater 2:397–401
6. Kaplan B, Groult H, Barhoun A, Lantelme F, Nakajima T, Dupta V, Komaba S, Kumagai N (2002) J Electrochem Soc 149(5):D72–D78
7. Kilby KT, Jiao S, Fray DJ (2010) Electrochim Acta 55:7126–7133
8. Jiao S, Fray DJ (2010) Metall Mater Trans B 41:74–79
9. Yin H, Gao L, Zhu H, Mao X, Gan F, Wang D (2011) Electrochim Acta 56:3296–3302
10. Tang D, Xheng K, Yin H, Mao X, Sadoway DR, Wang D (2018) Electrochim Acta 279:250–257
11. Massot L, Cassayre L, Chamelot P, Taxil P (2007) J Electroanal Chem 606:17–23
12. Kim H, Paramore J, Sadoway DR (2011) J Electrochem Soc 158:101–105
13. Kim SW, Choi EY, Park W, Im HS, Hur JM (2015) Electrochem Commun 55:14–17
14. Snook GA, McGregor K, Urban AJ, Lanyon MR, Donelson R, Pownceby MI (2016) R Soc Chem 190:35–52
15. Chen GZ (2020) Int J Miner Metall Mater 27:1572
16. Pasquet I, BacoGarles V, Chamelot P, Gibilaro M, Massot L, Tailhades PH (2020) J Mater Process Technol 278:116452
17. Bongio EV, Black H, Raszewski FC, Edwards D, Maconville CJ, Amarakoon VRW (2005) J Electroceram 14:193–198
18. Shimony U, Knuddsen JM (1966) Phys Rev 144:361
19. Sagdahl LT, Einarsrud MA, Grande T (2000) J Am Ceram Soc 83(9):2318–2320
20. Smolin SY, Scafetta MD, Choquette AK, Sfeir MY, Baxter JB, May SJ (2016) Chem Mater 28(1):97–105
21. Sasamoto T, Mizusaki J, Yoshimura M, Cannon WR, Bowen HK (1982) J Am Ceram Soc 65(8):363–368
22. Sata N, Ikeda K, Iguchi F, Yugami H (2007) Solid State Ion 178:1563–1567
23. Kado Y, Goto T, Hagiwara R (2008) J Chem Eng Data 53:2816–2819
24. Goto T, Araki Y, Hagiwara R (2006) J Electrochem Soc Electrochem Solid-State Lett 9(2):D5–D7
25. Kado Y, Goto T, Hagiwara R (2009) J Electrochem Soc 156(11):E167–E170
26. Kanzaki Y, Kogawa K, Yano S, Matsumoto O, Takahashi M (1975) DENKI KAGAKU 43(5):278–280

Authors and Affiliations

Shunichi Kimura[1] · Takashi Fukumoto[1] · Yuta Suzuki[1] · Takuya Goto[1]

✉ Takuya Goto
tgoto@mail.doshisha.ac.jp

[1] Department of Science of Environment and Mathematical Modeling, Graduate School of Science and Engineering, Doshisha University, Kyotanabe-shi, Kyoto 610-0394, Japan